AIAA JOURNAL
Vol. 39, No. 7, July 2001

Fluorescence Velocimetry of the Hypersonic, Separated Flow over a Cone

P. M. Danehy,* P. Mere,† M. J. Gaston,‡ S. O'Byrne,§ P. C. Palma,¶ and A. F. P. Houwing**
Australian National University, Canberra, Australian Capital Territory 0200, Australia

Planar laser-induced fluorescence of nitric oxide is used to measure a component of the velocity field for the Mach 7 flow around a 30-deg half-angle, 50-mm-diam cone mounted to a long, 38-mm-diam shaft, or "sting." Transverse velocities are measured in the freestream, the shock layer, and the separated region at the junction between the cone and the sting. For most of the flowfield, the uncertainty of the measurements is between ± 50 and ± 100 m/s for velocities ranging from − 300 to 1300 m/s, corresponding to a minimum uncertainty of ± 5%. The measurements are compared with the commercial computational fluid dynamics (CFD) code CFD-FASTRAN™. The agreement between the theoretical model and the experiment is reasonably good. CFD accurately predicts the size and shape of the shock layer and separated region behind the cone as well as the magnitude of the gas velocity near the reattachment shock. However, the magnitude of the velocity in the shock layer and gas expansion differ somewhat from that predicted by CFD. The discrepancies are attributed to a small systematic error associated with laser-beam attenuation and also to inexact modeling of the flowfield by CFD.

I. Introduction

EXPERIMENTAL simulation of hypersonic gas flows in a controllable environment can provide valuable information for designing hypersonic vehicles. Consequently, the development of accurate measurement techniques for use in hypersonic facilities holds considerable interest for the aerospace community.

Making nonintrusive velocity measurements in hypersonic shock-layer flows is particularly useful because they help quantify the distribution of kinetic energy throughout the flowfield. This is important because kinetic energy can be converted to thermal energy (by shock waves, expansions, or viscous effects) or chemical energy (by dissociation or combustion). These processes have important aerodynamic and heat transfer implications for aerospace vehicles. Thus, the velocity field provides an important comparison point between experiment and theory. Because of the complex nature of the flows being studied, theoretical predictions of hypersonic flowfields are usually provided by computational fluid dynamics (CFD) codes.

The hypersonic flow around a cone, including the separated region behind the cone, is a classic fluid mechanical problem. A critical dimension of this flowfield is the distance of the reattachment point from the base of the cone in relation to the height of the cone step. This is an important parameter for designers of reentry vehicles because insufficiently shielded payloads placed at the reattachment point can be damaged by excessive heating. To our knowledge, the velocity field of this hypersonic flow has not previously been studied experimentally. As already stated, velocity is an important parameter to measure in this flow because it provides information about the distribution of kinetic energy in the flow. We plan to complement this dataset with temperature measurements that describe the distribution of thermal energy of the flowfield. Velocity measurements also provide information about the slight divergence of the freestream gas, which is important for CFD modeling of the flowfield.

Physical probes, such as hot-wire anemometers, are inappropriate for studying supersonic or hypersonic flows because they disturb the flow. Furthermore, imaging methods are preferred to single-point methods, such as laser Doppler velocimetry (LDV), because the limited test time of the facility would make it very expensive to map the flow velocity.

Several laser-based methods have been developed for mapping the velocity in gaseous flows. These include particle image velocimetry (PIV), planar Doppler velocimetry (PDV),[1,2] Rayleigh scattering velocimetry,[3–5] and planar laser-induced fluorescence (PLIF) velocimetry. Particle-based velocimetry methods (PIV and PDV) are unattractive in supersonic flows because the particles do not follow the flow when steep velocity gradients, such as those resulting from oblique shock waves, are present. Rayleigh scattering velocimetry is a sensitive method that was considered carefully in the present study. However, preliminary measurements in our shock-tunnel facility showed that Mie scattering (from particles) overwhelmed Rayleigh scattering (from molecules) by more than an order of magnitude. A molecular absorption filter is commonly used to separate Mie and Rayleigh signals. However, we cannot use an absorption filter because in the present experiment both particles and molecules were moving at hypersonic velocities in some parts of the flow, and subsonic velocities elsewhere. Without a way to separate the Mie and Rayleigh signals in this flow, we abandoned that approach in favor of PLIF velocimetry. While PLIF has a lower sensitivity to velocity compared with PDV or Rayleigh scattering velocimetry, it has been used previously in our facility for measuring other parameters, such as temperature and species density, providing excellent signal-to-noise ratios. In this paper, we acquire PLIF images at multiple laser frequencies near an isolated spectroscopic transition and then process the images to determine the flow velocity from the observed Doppler shift.

II. Theory

A. Fluid Mechanics

In this paper, we study the hypersonic flow over a cone, illustrated schematically in Fig. 1. The hypersonic flow is produced by a free-piston shock tunnel. The cone simulates an aerospace vehicle carrying a payload, which is represented by the "sting" (the shaft holding the cone). Gas approaching the model from the freestream passes through a shock wave that turns the gas away from the cone while increasing its temperature and density and reducing its speed.

Received 4 January 2000; revision received 12 January 2001; accepted for publication 31 January 2001.

*Lecturer, Physics Department, Faculty of Science; currently Research Scientist, Mail Stop 236, NASA Langley Research Center, Hampton, VA 23681-2199; P.M.Danehy@larc.nasa.gov. Member AIAA.

†Honors Student, Physics Department, Faculty of Science.

‡Ph.D. Student, School of Aerospace and Mechanical Engineering, University College, Australian Defence Force Academy; currently Research Associate, Faculty of Engineering, University of Technology, Sydney, New South Wales 2007, Australia.

§Ph.D. Student, Physics Department, Faculty of Science. Student Member AIAA.

¶Research Associate, Physics Department, Faculty of Science; currently Research Scientist, German Aerospace Center, DLR, Bunsenstrasse 10, 37073 Göttingen, Germany. Member AIAA.

**Reader, Physics Department, Faculty of Science. Member AIAA.

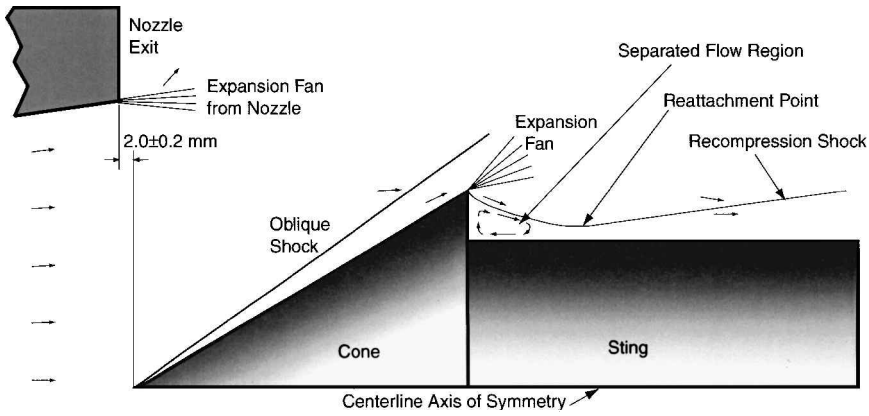

Fig. 1 Hypersonic gas flow over a sharp cone.

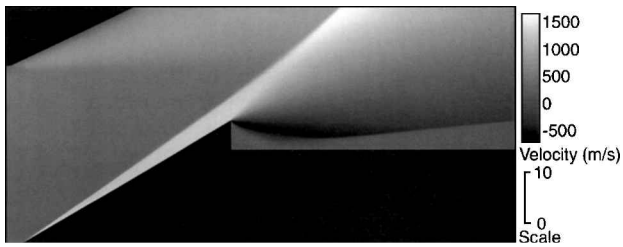

Fig. 2 CFD prediction of radial component of the velocity field.

When the gas reaches the expansion fan, it is accelerated back toward the flow axis, and its temperature and density are reduced. The gas from the shock layer cannot sharply turn around the shoulder of the corner. Instead, the flow separates from the model and reattaches on the sting farther downstream at the reattachment point.[6] The presence of the subsonic boundary layer on the sting prevents the reattachment shock from forming directly on the sting.

We have used the commercial CFD code CFD-FASTRAN™ to predict the radial component of velocity.[7] To simulate the diverging flow in the freestream, we started the simulation from the throat of the conical nozzle and assumed steady flow. We used the Roe's flux differencing scheme with the min-mod flux limiter to achieve second-order spatial accuracy. This Navier–Stokes code uses Sutherland's viscosity model and the ideal gas law to compute the gas density. The ratio of the specific heats was assumed to be 1.4. We used 132,364 grid cells in the computation. We expect the flow over the cone to be laminar, whereas the boundary layer in the nozzle is expected to be transitional. Unfortunately, because CFD-FASTRAN does not allow both laminar and turbulent flow in the same computational domain, we were required to assume laminar flow throughout the flowfield. As will be discussed later, this caused the expansion wave from the end of the nozzle to be poorly predicted by CFD. Another limitation of CFD was that the grid spacing on the back surface of the cone were spaced widely to stay within the limited amount of memory available.

Figure 2 shows the predicted radial component of the velocity field for the flow over the cone. The black region in the upper-left-hand corner of the image simulates the nozzle exit. To avoid the time-consuming computation of a second separated flow region, the exit of the nozzle is modeled as a nonseparating expansion (Fig. 2). In reality, the nozzle terminates abruptly at 90 deg to the flow axis, as shown in Fig. 1. The model is shown in black in the bottom right of the image. On the centerline, the freestream gas has an axial velocity of 3000 m/s and has no radial component. The shock wave forming on the tip of the cone interacts with the expansion wave from the nozzle, causing the shock to bend slightly away from the model at the top of the image. Inside the shock layer, the radial velocity is ~1200 m/s. The maximum radial velocity, in excess of 1600 m/s, is located at the top of the image, just past the shock wave. The gas inside the shock layer and close to the model expands around the shoulder of the cone, resulting in a large (~800 m/s) radial velocity toward the model. Finally, the recompression shock forces the flow parallel to the sting, resulting in a near-zero velocity near the sting. The velocity map clearly shows the separated flow region, inside which the gas has near-zero velocity.

B. Fluorescence Velocimetry

We use PLIF to measure the velocity field. PLIF is now a well-established flow imaging technique for measuring velocity as well as temperature and pressure.[8] For several years, we have used PLIF in hypersonic shock layer, supersonic combustion, and hypersonic mixing studies.[9–11] The PLIF method uses a pulsed, tunable laser to generate a beam that is collimated into a thin sheet that illuminates a planar cross-section of the flowfield. This light is absorbed by some of the molecules in the flow, and the resulting fluorescence is detected by an intensified digital camera providing visualization and quantitative measurements of the flowfield in the cross-section.

PLIF velocimetry methods have been developed using both the Doppler shift between the moving molecules and the incoming laser beam[12–19] and flow tagging,[20–22] in which time-of-flight of laser-excited molecules is used to determine the flow velocity. Compared with Doppler-based PLIF velocimetry, flow-tagging methods are generally more sensitive to low velocity flows. However, Doppler-based methods provide two-dimensional maps of the flow velocity, whereas flow-tagging methods usually measure velocity along a line or lines. Furthermore, flow-tagging methods usually require two independently tunable and delayable pulsed lasers, whereas Doppler-based methods require only a single tunable laser.

The current experiment uses a variation of the Doppler-shift-based velocimetry method demonstrated by McDaniel et al.[14] and subsequently used by Palmer and Hanson,[16] Donohue and McDaniel,[23] Klavuhn et al.,[19] and others. Whereas McDaniel et al. used a continuous-wave laser in a continuous-running facility, we used the approach of Palmer and Hanson, in which PLIF images are obtained with a pulsed laser on multiple runs of a shock tunnel. In an approach similar to that of Klavuhn et al.,[19] we obtained a series of images with slightly different laser frequencies near a single, isolated, nitric oxide absorption transition. Through image processing, we measure the absorption line shape at each point in the flowfield. The Doppler shift, and then the flow velocity, are obtained from this absorption spectrum.

Two different types of instantaneous Doppler-based velocimetry methods have been developed by others using PLIF. The two methods rely on the laser linewidth ($\Delta\nu_L$) being much broader than,[17] or much narrower than,[13] the transition's absorption linewidth ($\Delta\nu_T$) throughout the flowfield. However, a significant complication in the current experiment is that the pressure and temperature variations throughout the image are large, ranging from 5 kPa and 400 K in the freestream to approximately an atmosphere and 1600 K in the shocklayer region. This range of conditions causes significant collisional broadening and shift as well as Doppler broadening of the nitric oxide transitions.

In the current experiment, the transition linewidth varies from ~0.12 cm^{-1} in the freestream to ~0.27 cm^{-1} in the shock layer. To use the method that assumes $\Delta\nu_L \gg \Delta\nu_T$ would have required a laser linewidth of ~3 cm^{-1} in the ultraviolet, which is not commercially available. On the other hand, because of the large range of velocities

in the current experiment (~1500 m/s), the range of Doppler shifts is ~0.22 cm^{-1}. Therefore, if the method that assumes $\Delta\nu_L \ll \Delta\nu_T$ was used, parts of the image would have no fluorescence intensity because the transition would have shifted completely off the line. This would cause inaccurate or anomalous velocity measurements. Thus, using commercially available pulsed lasers, we could not measure the velocity field instantaneously. Instead, we have used a laser with a linewidth of 0.18 cm^{-1} to directly measure the average transition lineshape on multiple runs of the tunnel.

Faced with a similar problem, Allen et al.[18] developed an algorithm to determine velocity by analogy to the $\Delta\nu_L \gg \Delta\nu_T$ and $\Delta\nu_L \ll \Delta\nu_T$ methods. This technique allows the velocity field to be measured with a single laser pulse, but it is susceptible to errors if the flow conditions vary greatly throughout the flowfield. They demonstrated that the method works reasonably well for flows near atmospheric pressure with moderate (up to a factor of ~4) changes in pressure. However, in the current experiment, the pressure varies by almost two orders of magnitude in the imaged region, which causes significant collisional shifts that would lead to large systematic errors if this method was used.

In the present paper, Doppler-based PLIF velocimetry has been adapted to the harsh environment of a free-piston shock tunnel. The method makes no assumptions about either the spectral profile of the laser or the absorption transition. Instead, the entire fluorescence spectrum is measured at each point in the flow. As shown in Fig. 3, we align the laser sheet so that it passes just beneath the sting and continues on through the flow on the opposite side of the model. As a result of the axial symmetry of the model and flow, the flow on one side of the sting is the mirror image of that on the other side. The Doppler shift with respect to the laser is equal in magnitude but opposite in direction for points on opposite sides of the axis of symmetry. We use this flow symmetry to separate out the collisional shift from the Doppler shift.

Figure 4 shows how the velocity is recovered from these images. Multiple fluorescence images are obtained using various laser frequencies near an isolated absorption transition. At each point in the flowfield, the fluorescence intensity is plotted as a function of excitation frequency. A Gaussian curve is fit to the data, using the method of least squares. The center of the fitted Gaussian is used as an estimate of the transition line center. The choice of a Gaussian, as opposed to a Lorentzian or Voigt, profile is not important, because each would locate the line center of the spectrum equally well. A Gaussian was chosen for computational efficiency.

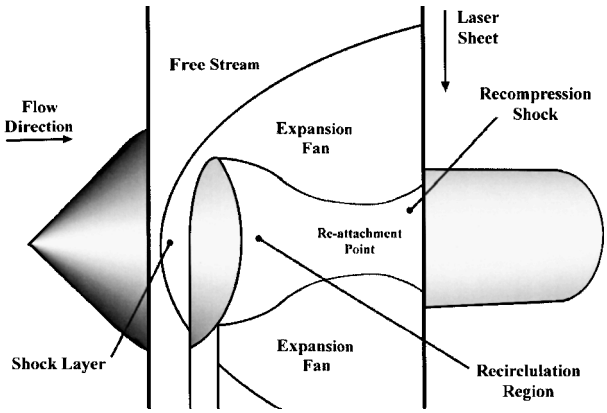

Fig. 3 Orientation of the laser sheet relative to cone as viewed from below.

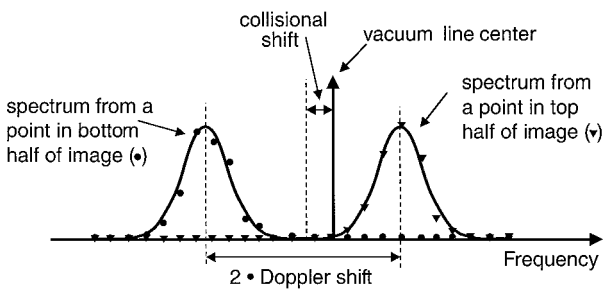

Fig. 4 Pictorial description of PLIF velocimetry method.

Locating the center of the transition allows us to determine the sum of the collisional and Doppler shifts at each point in the image. The collisional and Doppler shifts can be as large as 0.06 and 0.22 cm^{-1}, respectively, in the present experiment. Next, we invoke flow symmetry and assume that the collisional shift is the same at points reflected across the flow centerline. As shown in Fig. 4, the difference in frequency between the two transition line centers is twice the Doppler shift, $\Delta\nu_D$. Finally, the Doppler shift can be related to the component of the flow velocity toward the laser, V, using the relationship

$$V = c\Delta\nu_D/\nu_L \tag{1}$$

where c is the speed of light and ν_L is the laser frequency.

III. Experiment

The experiments were performed on the T2 free-piston shock tunnel at the Australian National University.[24] A schematic of the experiment is shown in Fig. 5. The nozzle has a 15-deg full-angle conical geometry with a 6.4-mm-diam throat and a 73-mm exit, resulting in an exit-to-throat-area ratio of 144. The nozzle had a throat-to-exit length of 255 mm. The shock tube was filled with a mixture of 98.9% N_2, 1.1% O_2 to 100 kPa and was at room temperature before tunnel operation. This gas mixture was chosen to produce an amount of NO that was substantial enough to produce good fluorescence images, but not so much that the laser is absorbed substantially as it passes through the flow. The primary shock speed was 2.4 km/s, which corresponds to a flow enthalpy of 5.3 MJ/kg. The nozzle-reservoir pressure was measured to be 27.9 MPa, and reservoir temperature was calculated to be 4219 K using the equilibrium shock-tube code, ESTC.[25] We used the one-dimensional nonequilibrium code STUBE to estimate the nozzle-throat conditions (to be used as an inlet condition for CFD-FASTRAN) and to estimate the freestream conditions.[26] At the nozzle throat, STUBE predicts that the velocity is 1.23 km/s, the temperature is 3650 K, and the pressure is 14.2 MPa. At a distance of 285 mm from the nozzle throat, the calculated freestream temperature, pressure, Mach number, and velocity were 396 K, 4.4 kPa, 7.7, and 3.0 km/s, respectively. The estimated gas composition at this location was 98.1% N_2, 1.1% NO, 0.4% O_2, and 0.3% O.

During the measurement time, the tunnel recoils 8.0 ± 1.0 mm. After recoil, the tip of the cone was located 2.0 ± 0.2 mm outside the nozzle, corresponding to a distance of 257 mm from the nozzle throat. The cone was 44.0 mm long and had a 25.4-mm radius. The step height behind the cone was 6 mm. The radius of the sting was therefore 19.4 mm. The laser sheet was centered 0.5 ± 0.3 mm above this and was measured to be 0.8 ± 0.1 mm thick.

We frequency-doubled the output of an excimer-pumped dye laser (Lambda Physik; Scanmate II) to obtain up to 5-mJ, 25-ns pulses at 225 nm, coinciding with the (0,0) vibrational band of the $A - X$ electronic transition of NO. Most of the laser light was formed into a sheet 80-mm wide and was directed into the test section perpendicular to the flow. Less than 1 mJ was used to form the laser sheet, resulting in low intensity that reduced power broadening of the transitions. A small portion of the laser beam was split off and used for wavelength calibration by performing LIF in a gas cell filled with a small quantity of NO together with a few kPa of N_2. Previously, the laser linewidth was measured to be 0.18 ± 0.01 cm^{-1} based on LIF measurements in the same gas cell.[11] This is consistent with specifications from the manufacturer.

We adjusted the laser to a specified frequency near an NO transition before each run of the shock tunnel. Immediately before the shot (<5 s), the tunnel operator stopped the laser via a remote switch next to the firing valve. After the firing valve was opened, the nozzle reservoir pressure transducer detected the shock reflection at the end of the shock tube and the laser fired 350 μs later. This delay was chosen to coincide with the period of steady flow in the shock tube. An intensified charge-coupled device (CCD) camera (ICCD; Princeton Instruments; 16-bit CCD, 576 × 384 pixels, 50-ns gate duration) captured the fluorescence image at right angles to the laser sheet.

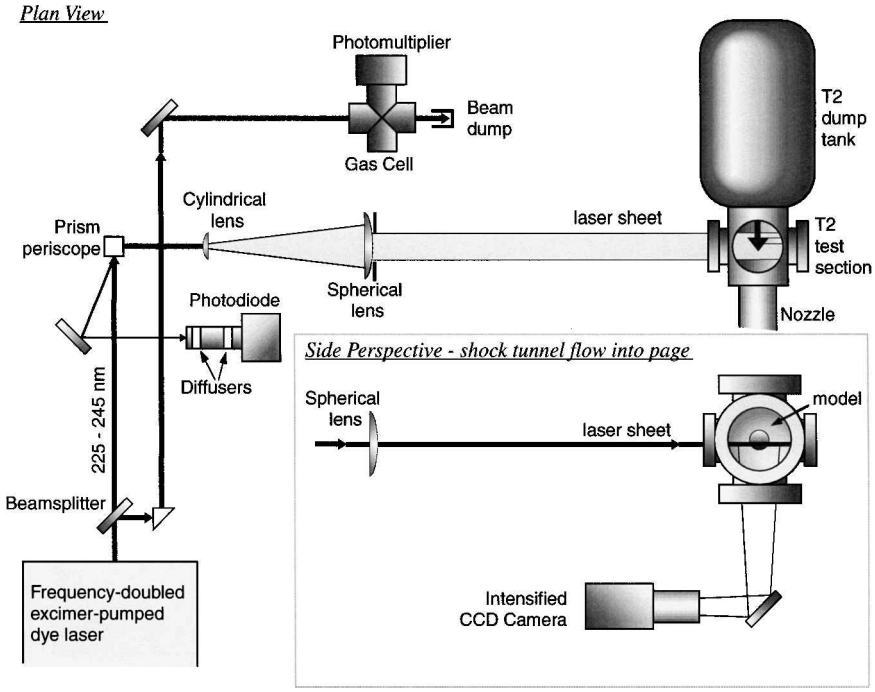

Fig. 5 Experimental setup used for velocimetry.

The image resolution was 5.8 pixels per mm. A 2-mm-thick UG-5 filter was placed in front of the ICCD camera. This filter allowed the fluorescence above 230 nm to pass into the camera but cut off most of the scattered laser light and some of the flow luminosity. The filter also blocked resonant fluorescence [$A - X$ (0, 0) near 226 nm], which reduced the influence of radiative trapping.

We probed the $R_2(20.5)$ transition of NO at 44,327.85 cm^{-1}. This transition was chosen for its appreciable ground-state population for all temperatures expected in the experiment as well as isolation from other transitions; the nearest transition is ~2 cm^{-1} away. Absorption of the laser sheet on its passage through the flow was ignored in the analysis. The maximum level of absorption was predicted to be around 8% per cm inside the shock layer when the laser is tuned to transition line center and significantly lower elsewhere. As discussed later, absorption causes a small systematic error in the measurement, but this error has been kept small by probing a relatively weak transition and by choosing a test gas composition with a relatively small quantity of NO (compared with using air as the test gas). Considering the laser energy used, the pulse duration, the beam area, the transition line strength, and an estimate of the flow conditions, we predict that the laser irradiance is only 10% of the saturation irradiance (I_{sat}) in the freestream and lower elsewhere, except in the recirculation region, where it is probably a factor of two higher. The discussion in Sec. IV explains that transition saturation does not cause systematic errors in determining the velocity using this method.

IV. Analysis and Results

Thirty experimental PLIF images were obtained. A sample of four of the raw images is shown in Fig. 6, labeled by the laser detuning in cm^{-1} relative to vacuum line center. Flow is from left to right, and the laser sheet enters from the top of each image. Two shadowed regions appear as vertical lines in the images. The thicker shadow at the bottom of each image is where the cone itself has blocked the laser sheet. The thinner shadow at the top of each image was caused by a small mask inserted to block the beam, preventing a large amount of laser light from reflecting off the model and damaging the ICCD camera. The leftmost part of each image shows the freestream gas. The gas in the freestream is diverging slightly, owing to its continued expansion from the conical nozzle. The gas then passes through the shock layer, and then to the expansion, beginning at the shoulder of the cone. Finally, the gas passes the recirculation region and continues through the recompression shock, all of which are clearly visible in the images. The graphs at the right of the raw images show vertical profiles through the images taken near the reattachment point. These graphs further illustrate the change in fluorescence intensity across the image: regions of the flow where the combination of Doppler and collisional shifts match the laser frequency have larger fluorescence intensities.

The raw images were corrected for camera dark current and offset, residual scattered laser light and flow luminosity, spatial variations in the laser-beam profile, overall laser intensity, and a slight camera movement that occurred on each tunnel run. To increase the speed of the analysis and to reduce the noise in the calculated velocities, the pixels of the processed images were binned 3 × 3, creating a reduced number of "superpixels." These images were written to text files and were imported to a spreadsheet where all images could be accessed simultaneously.

The spectral shift at each point in the flow was computed by fitting a Gaussian line shape to the spectra, as described in Fig. 4. Figure 7 shows some typical experimental spectra and Gaussian fits to the data from three different regions of the flow. We attribute the significant noise in the measurements to randomly varying flow luminosity, shot-to-shot fluctuations in the laser's spectral profile,[27] and, to a lesser extent, the imperfect reproducibility of the shock-tunnel conditions. Each spectrum contains information from 9 CCD pixels and 30 tunnel runs. The Doppler shift is determined from the difference in the fitted transition line centers for points on opposite sides of the symmetry axis. The component of the velocity in the direction of the laser is then computed using Eq. (1). The collisional shift can be determined from the average frequency line center for points on opposite sides of the flow axis, compared to the vacuum line center.

Figure 8 displays the resulting velocity map. The top half of the figure shows the experimental velocity map, and the bottom half shows the corresponding CFD velocity map, computed using the commercial program CFD-FASTRAN, described in Sec. II.A. In both cases, the velocity shown is the component of the velocity in the direction of the laser sheet. It is remarkable how smooth the measured velocity profile is, considering the quality of the spectra from which it was determined.

The measurements confirm that the freestream flow is diverging (velocity increasing away from the center of the image, which is the axis of symmetry). This flow divergence is caused by using a conical nozzle. We chose a conical instead of a contoured nozzle to avoid the centerline focusing effects that occur when contoured nozzles are operated away from design conditions. As expected, inside the shock layer, gas at the flow centerline approaches zero

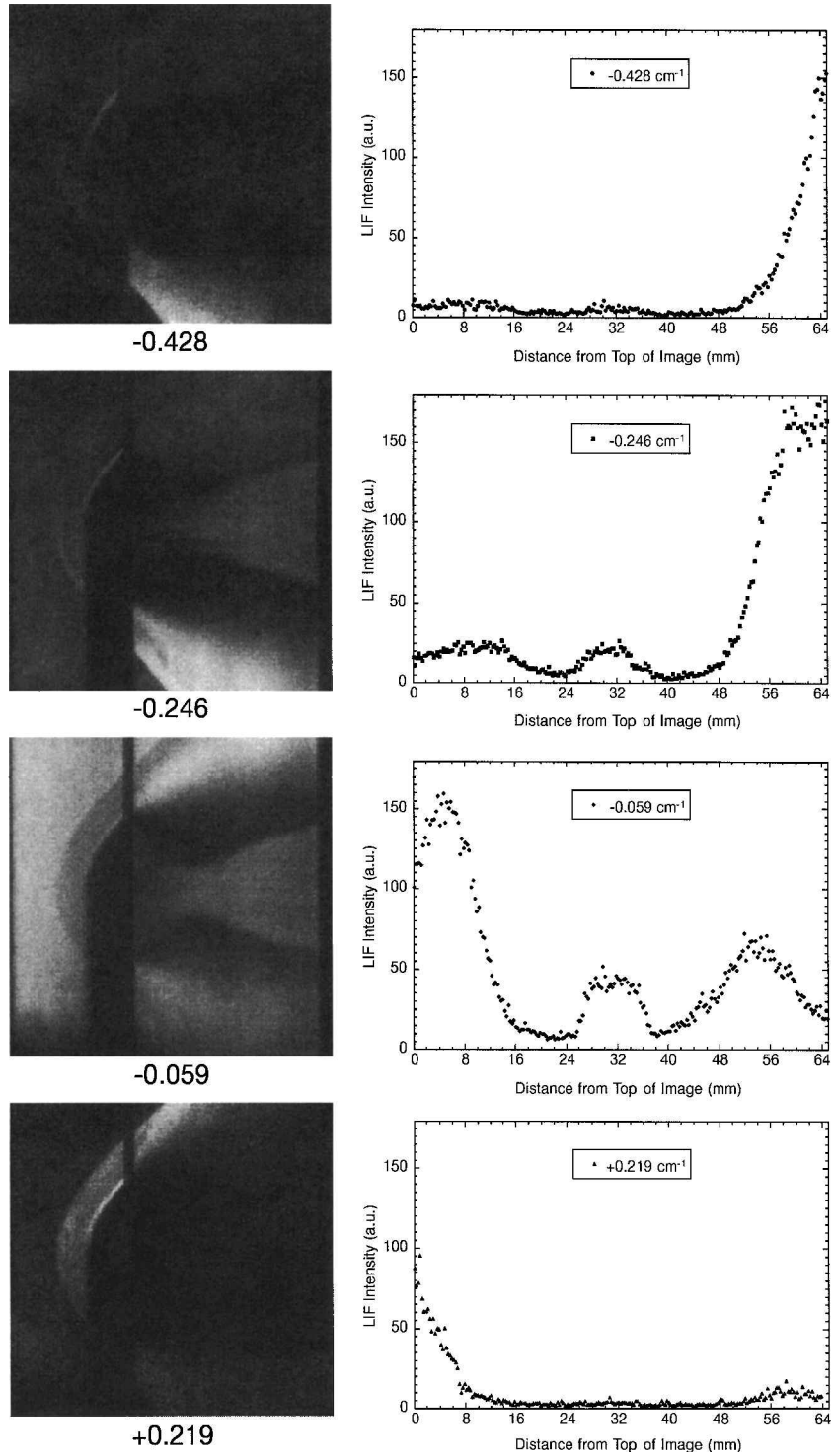

Fig. 6 Four typical fluorescence images obtained at different laser tunings on subsequent tunnel runs. The laser frequency relative to vacuum line center is indicated (in cm^{-1}) below each image. The graphs on the right are vertical profiles through the images near the reattachment point, 10 mm downstream of the step.

velocity in the direction of the laser sheet. It accelerates toward the laser as it moves farther away from the centerline. The maximum velocity is achieved in the outermost part of the shock layer, where the freestream gas has a substantial (~600 m/s) radial component even before it passes through the shock. As the gas expands around the shoulder of the cone, it achieves a negative velocity relative to the laser sheet. Inside the separated flow region immediately at the base of the cone, the velocity decreases because of viscous interactions in the shear layer and the adverse pressure gradient generated by the reattachment shock. In most of this region, the flow is subsonic and has a very small radial velocity component.

Potential sources of systematic errors in this experiment include laser beam attenuation, transition saturation, finite laser linewidth, and radiative trapping. However, considering each of these error sources in detail shows that only laser beam attenuation causes a significant systematic error in the current experiment. When the laser beam is resonant with molecules in the top half of the imaged flow, light is absorbed and the beam is attenuated. This causes the fluorescence to be artificially low in the bottom half of the flow in images where the laser is resonant with molecules in the top half of the flow. This would cause the line shape obtained from the bottom half of the images to be shifted slightly compared with where it would be in the absence of absorption. The measured velocities are then systematically large where laser attenuation has occurred. We have modeled this process and predict that in the shock layer, where the absorption is the greatest (8% per cm, over a distance of 2 cm),

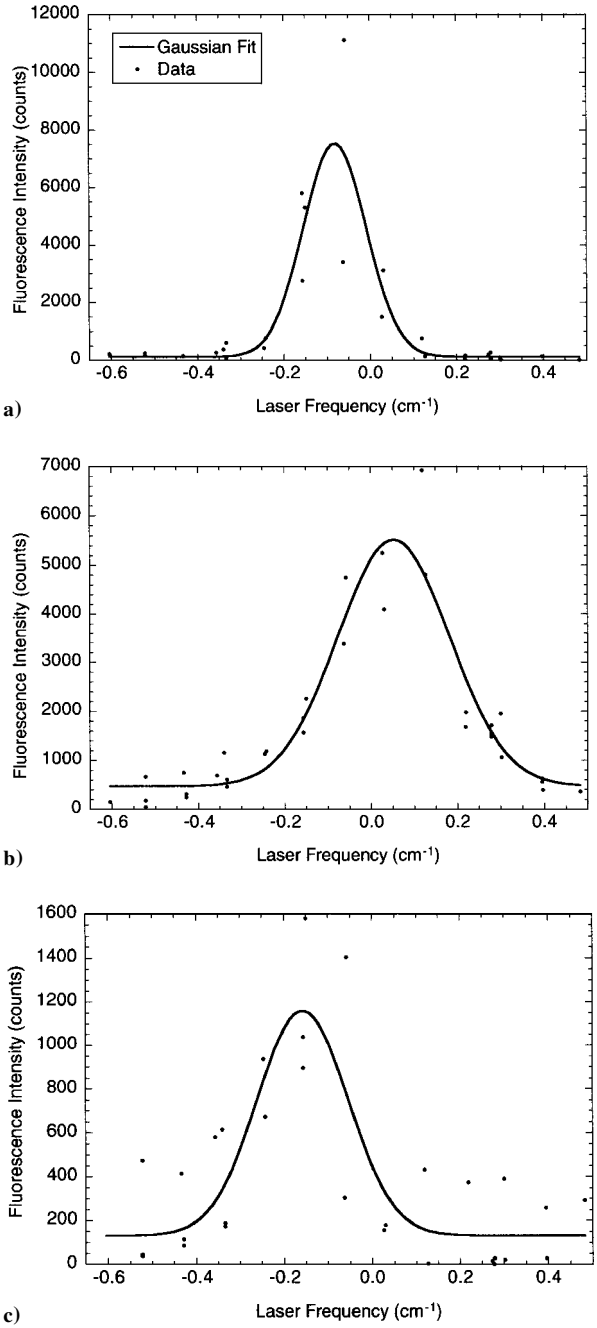

Fig. 7 Typical excitation spectra obtained from fluorescence images. These spectra show fluorescence intensities at a single location (pixel) in each of 30 images on 30 successive tunnel runs. The spectra were obtained from the a) freestream, b) shock layer, and c) recirculation region.

the measured velocities are systematically large by 60 m/s, at most (see error bar on Fig. 9b. Near the axis of symmetry, the error tends to zero. Also, in regions of the flow such as the freestream, where absorption is negligible, the error is negligible (<3 m/s). Finally, regions of the flow where the Doppler shift is large compared with the transition width, such as in the expansion region, the error is negligible (<15 m/s). Thus, the error caused by laser attenuation is substantial only in the shock layer on the cone.

On the other hand, transition saturation does not cause a systematic error in the velocity measurement. Saturation would broaden the spectral lines, possibly by different amounts at various locations throughout the flowfield, but the center position of each absorption transition would be unchanged. The laser linewidth, which is broader than the transition linewidth in some parts of the flowfield, acts to broaden the spectral absorption features, but again it does not systematically change the measured velocities. These three effects (laser attenuation, transition saturation, and using a broad laser linewidth) all act to broaden the observed spectral lines, which reduces the sensitivity of the velocimetry method. Consequently, in the present experiment, saturation was avoided by using relatively low laser intensities, and absorption was minimized by using a gas mixture containing only a small quantity of nitric oxide. In the present experiment, radiative trapping has been avoided by using a UG-5 filter in front of the camera, which blocks fluorescence at 225 nm from molecules returning to the ground electronic and vibrational state.

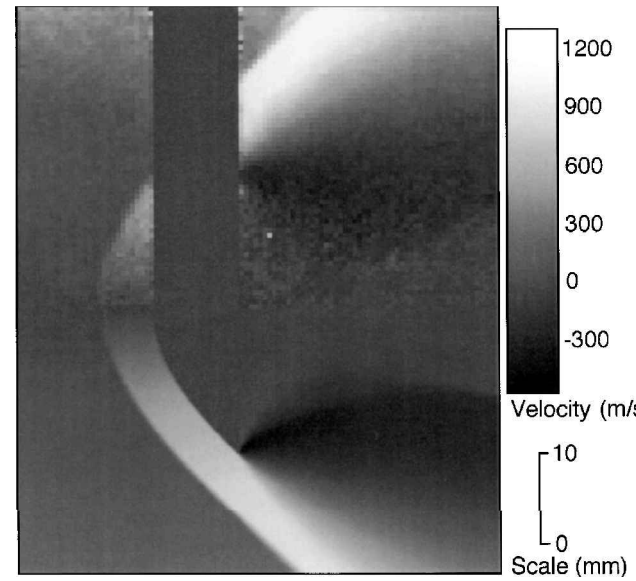

Fig. 8 Comparison of the experimental (top) and theoretical (bottom) velocity maps.

Possible sources of random error include shot-to-shot fluctuations in the laser's spectral profile and frequency, shot-to-shot variations in the operating conditions of the tunnel, and shot-to-shot variations in the luminosity from contaminants in the flow. All of these random fluctuations combine to make the spectra like those shown in Fig. 7 quite noisy. However, the Gaussian fit algorithm does an excellent job of computing sensible velocities from these noisy data: only a few clearly bad data points are seen in the velocity map. The best way to quantify these random uncertainties would be to perform the experiment many times and then measure the standard deviation of the resulting distribution of velocities. This approach is not feasible in the current experiment because it took approximately one week to acquire the data used to make this measurement. However, pixel-to-pixel variations in the velocity map provide a satisfactory source of data on which to base the uncertainty. We measured the standard deviation in small (20 to 40 superpixel) regions of the flow that had a relatively uniform velocity. Later, we state the uncertainty in the measurement as ± 2 standard deviations, so the true value is within the error bars with a confidence of 95%. Using this method, the uncertainties in the measured velocities in the freestream, shock layer, expansion, recirculation region, prereattachment shock, and postreattachment shock are ± 50, ± 70, ± 90, ± 100, ± 90, and ± 60 m/s, respectively. The uncertainty determined for the shock layer, where the largest measured velocity occurred, corresponds to a $\pm 5\%$ measurement uncertainty.

The uncertainty could be reduced substantially in the cooler, lower-pressure parts of the flow by using a narrower linewidth laser. Inserting an intracavity etalon into the dye laser used in this experiment would have decreased the laser's linewidth by a factor of four. Unfortunately, this etalon was not available for the current work. Such a laser would make the spectra like those shown in Fig. 7 narrower, making it easier to identify the center frequency. An added benefit of using a single-mode laser is that noise contributions from shot-to-shot variations in the laser's spectral profile would be significantly reduced or eliminated. Other strategies could be used to improve the measurement accuracy, as well. These include using a shorter gate time on the camera (say, 20 ns instead of 50 ns) to

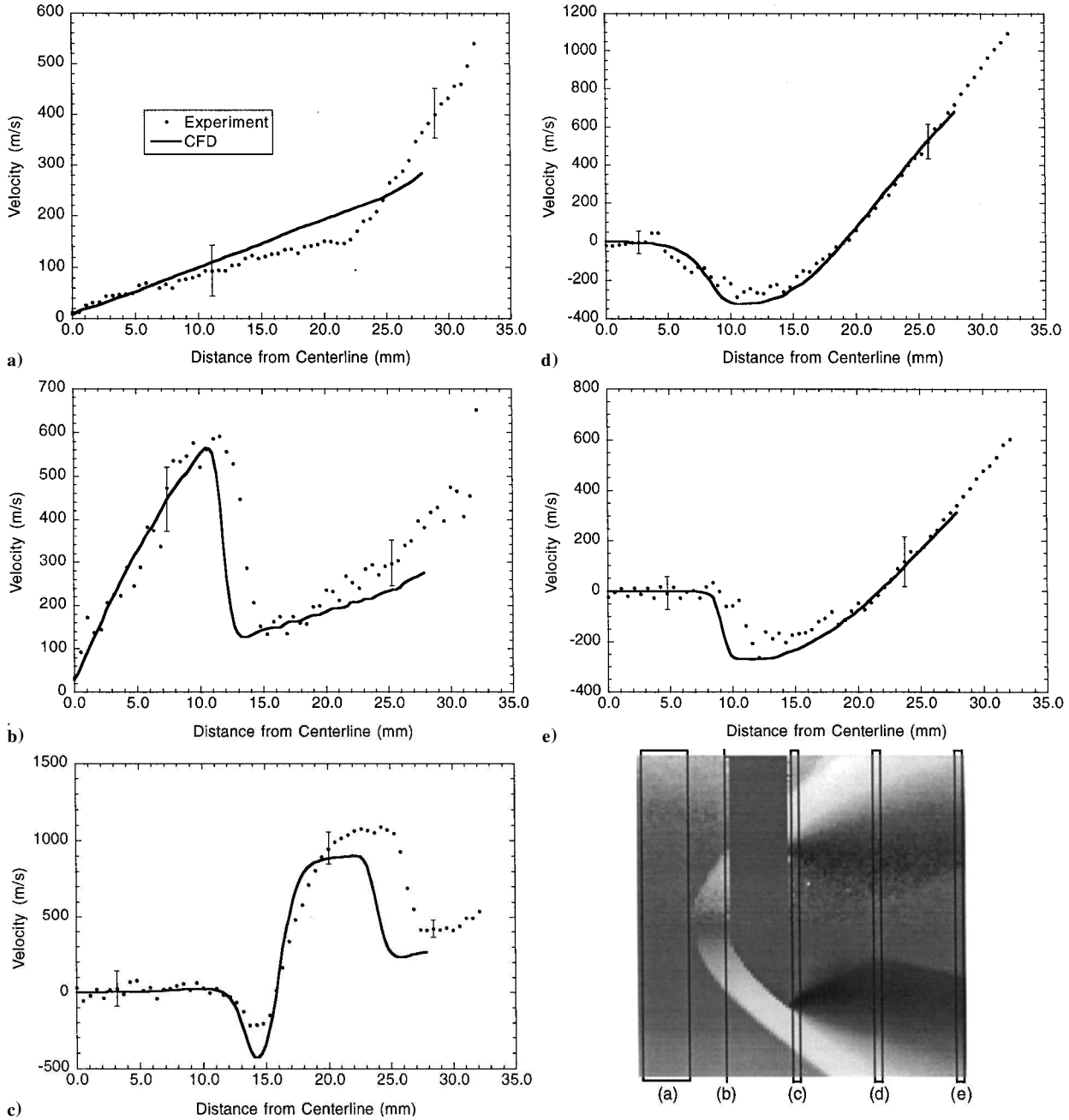

Fig. 9 Comparison of experimental and theoretical velocity profiles. The image in the bottom-right-hand corner shows where each profile is taken in the original velocity image.

reduce the flow luminosity. Alternately, the natural luminosity flow could be measured just before the laser pulse by using a second CCD camera. This luminosity would be removed from the PLIF images in subsequent image processing.

The computed and measured velocity maps agree well regarding the structure of the flow and the overall trends in the velocity field. The thickness and shape of the conical shock wave are in good agreement with CFD, although CFD slightly underpredicts the shock angle. Importantly, the size of the recirculation zone is in excellent agreement. This is in contrast with our first attempts at modeling this flow with the commercial software CFD-ACE,[7] for which only a first-order solution would converge. That computation resulted in a recirculation region that was half as large as that measured in the experiment. Finally, the location of the reattachment shock is in very good agreement in the two images. The most notable discrepancies between the two images is in the magnitude of the velocities measured in the shock layer and the expansion just past the shoulder of the cone.

Figure 9 shows quantitative comparisons between theoretical and experimental velocities. The graphic in the bottom-right-hand corner of the image shows where each cross-sectional cut was made in the velocity map. Figure 9a shows the velocity in the freestream, averaged in the streamwise direction over 16 superpixels, corresponding to 8 mm. In the central core of the flow, less than 15 mm from the centerline, the agreement between theory and experiment is excellent. However, the flow does not diverge as much as theory predicts between 15 and 23 mm from the centerline. Beyond 23 mm, there is a large discrepancy between theory and experiment. In the experimental image, the expansion wave originating from the nozzle exit is much stronger than in the CFD image, and it extends into the core flow much more than CFD predicts. Clearly, CFD is not perfectly modeling the flow at the edge of the nozzle exit. We think the flow is poorly modeled here because CFD assumed that the boundary layer on the nozzle wall was laminar, resulting in a very thin boundary layer at the exit. Had a turbulent boundary layer been used on the nozzle, the nozzle boundary layer would have been much thicker and the expansion wave would have protruded into the core flow farther upstream. Previous temperature measurements in the same facility at the same experimental conditions indicated that the measured boundary layer on the nozzle is thicker than that predicted

by a laminar CFD code[28] but not as thick as that predicted by a fully turbulent CFD code. Thus, we estimate that the nozzle flow is transitional. The best simulation of the nozzle flow would then be to have laminar flow for three-quarters of the nozzle (for example), followed by turbulent flow for the final one-quarter of the nozzle. Unfortunately, CFD-FASTRAN does not allow both turbulent and laminar flow regions in the same computation. So, using the current CFD code, we cannot improve this aspect of the computation.

Figure 9b shows the velocity profiles for a region 1 superpixel wide through the shock layer. Within the shock layer, the measured velocities agree with the computed velocities within experimental error. At distances far from the centerline, the experiment shows larger velocities than does CFD, probably owing to poor modeling of the boundary layer on the nozzle, as discussed.

Figure 9c shows a slice 3 superpixels wide located just past the cone shoulder. The location of the shear layer between the expanding gas and the recirculating gas is modeled accurately by CFD. However, CFD overpredicts the magnitude of the gas velocity in the expansion by a factor of two. We attribute this discrepancy to the coarse grid spacing near the cone shoulder, which forces the gas to overexpand in that region. Because we were limited by the amount of memory in the computer, we could not refine this grid further. The total maximum-to-minimum change in velocity in the CFD is very close to the experimental value. The magnitude of the predicted velocity in the postshock region (at 22 to 27 mm from the centerline) is too low by approximately 250 m/s. Again, this is attributed to inaccurate modeling of the nozzle boundary layer by CFD.

Figures 9d and 9e show 3-superpixel slices taken 15 and 28 mm downstream of the cone shoulder. The zero-radial-velocity region close to the sting confirms the reliability of this technique to accurately determine the flow velocity. On the other side of the reattachment shock, CFD is again in excellent agreement with the experiment. The position of the reattachment shock and shape of the velocity profiles are predicted very well by CFD.

V. Discussion

Hiller and Hanson[13] provided a very thorough discussion of the relative merits of fixed-laser-frequency vs tuned-laser-frequency schemes for measuring velocity. This section summarizes the issues relevant to the present experiment. Later in this section, we consider extensions of the current method for measuring other components of the velocity in the shock tunnel.

Fixed-frequency measurement schemes[12,13,16–18] have the ability to measure velocity instantaneously. This means they can be applied to study unsteady flows. Furthermore, instantaneous measurements are much cheaper when the flow facility run time is the largest expense, as is usually the case with large free-piston shock tunnels. However, tuned-frequency schemes such as the one presented in this paper have several advantages compared with fixed-frequency schemes. In particular, the range of velocities that can be measured with fixed-frequency schemes is limited by the linewidths of the laser and/or the absorption transition. This issue is particularly important in hypersonic flows, where the range of velocities can exceed 3000 m/s. Also, transition saturation and attenuation of the laser sheet by particle scattering and/or absorption, both of which are unavoidable in the current experiment, cause systematic errors in the velocity measurement in fixed-frequency schemes, whereas for tuned-frequency schemes they do not. Beam attenuation of as little as 5% across the image can cause major errors in determining the velocity in fixed–frequency arrangements.[13] The experimental procedure and data analysis are both much simpler for the tuned-frequency schemes. In general, fixed-frequency schemes result in lower accuracy and precision in the measured velocities.[13] In summary, whereas fixed-frequency schemes produce instantaneous velocity field measurements, tuned-frequency schemes like the one presented in this paper are, in general, simpler and more accurate.

The tuned-frequency scheme presented in this paper used one laser and one camera and determined one component of the velocity field by assuming a symmetric flowfield. With slightly more experimental effort, the assumption of a symmetric flowfield could be relaxed. For example, counterpropagating laser sheets[17] can be used to determine the component of the flow velocity in the direction of the laser sheet without assuming flow symmetry. The method could be extended to measure more components of the velocity field by directing additional laser sheets into the flowfield. For example, Hiller and Hanson directed four sheets into the flow at different angles to simultaneously determine the velocity and pressure in an underexpanded free jet.[13] Palmer and Hanson[16] provide a table summarizing the options for instantaneous velocity imaging using fluorescence. The table indicates how many velocity components can be obtained for a particular experimental configuration. Table 1 reproduces their table in part. Palmer and Hanson's analysis holds for the current experiment as well. However, in hypersonic flow facilities, the large range of velocities dictate that tuned-laser schemes should be used, resulting in time-averaged instead of instantaneous velocity measurements. Because the measurement is performed over many tunnel runs, measurements with different laser sheets can be obtained with a single camera. Yet, if multiple cameras are available, measurements can be obtained simultaneously, reducing the number of tunnel runs required. As Table 1 indicates, for the case of an arbitrary flowfield, laser sheets entering the flow from four directions are required to measure two components of the velocity field. However, extra considerations also must be taken into account, such as optical access to the flow and possible blockage of the laser sheets by the model.

Table 1 Velocity measurement options for planar laser-induced fluorescence[a]

Number of laser sheets	Symmetric flow assumed	Number of velocity components obtained
1	Yes	1
2	No	1
2	Yes	2
4	No	2

[a] All methods use a single tunable laser. After Palmer and Hanson.[16]

VI. Conclusions

For the first time, we have demonstrated fluorescence velocity measurements in a free-piston shock tunnel. The method used is robust and reliable, but it is also time consuming and, in its present form, requires flow symmetry. This method could be extended to measuring nonsymmetric flowfields by directing additional laser sheets into the flow. However, obtaining other components of the velocity field would be difficult in the present facility, where the optical access is very restricted.

The measured velocity map shows very good signal-to-noise ratio. Velocities between −300 and 1300 m/s were measured with uncertainties of better than ±100 m/s. The minimum uncertainty corresponded to ±5%. A comparison between the experimental velocity map and a computation showed good overall agreement. Most important, the computation correctly predicted the velocity components near the centerline in the freestream, shock layer, and recirculation zone and near the reattachment shock. Furthermore, we found good agreement between the size and shape of the recirculation region and reattachment point of the separated flow. Owing to limitations in the CFD code, the predicted flow velocity away from the centerline did not agree with measurements. Nonetheless, this experimental result should provide a reliable dataset against which hypersonic CFD codes can be tested. Such comparisons should be facilitated by the conversion algorithm shown in the appendix.

Appendix: Conversion of Radial to Off-Axis Velocities

This appendix briefly describes the algorithm for determining the flow properties from CFD for an off-axis planar slice through an axisymmetric flowfield. Two planes are defined. Plane 1 is the radial plane in which the axisymmetric CFD computation was performed. Plane 2 is the off-axis plane in which the measurement was performed. Plane 2 passes a distance h away from the centerline. This algorithm converts predicted velocities in plane 1–2.

First, y-pixel positions must be defined in plane 2. These are represented by evenly spaced dots in Fig. A1. Then the radius r can be computed from $r = \sqrt{(h^2 + y^2)}$. Interpolation must then be used to determine the radial velocity (V_{radial}) in plane 1 predicted by CFD

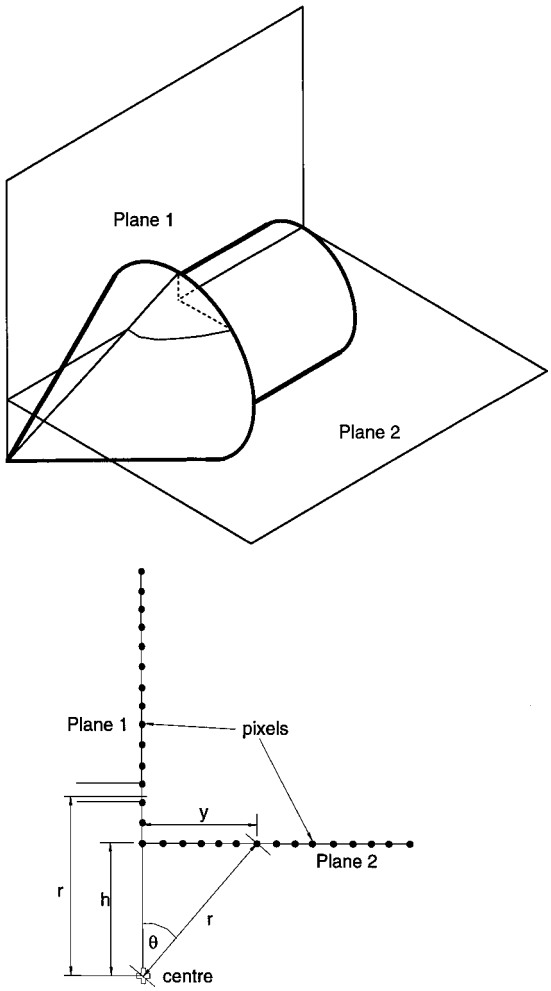

Fig. A1 Diagram explaining algorithm for converting predicted radial velocities to an off-axis plane.

at a distance r from the centerline. Finally, the component of the velocity in the direction of the laser sheet, at the position y in plane 2, can be determined from $V = V_{\text{radial}}(y/r)$.

References

[1]Mosedale, A. D., Elliot, G. S., Carter, C. D., Weaver, W. L., and Beutner, T. J., "On the Use of Planar Doppler Velocimetry," AIAA Paper 98-2809, June 1998.

[2]Clancy, P. S., Samimy, M., and Erskine, W. R., "Planar Doppler Velocimetry: Three-Component Velocimetry in Supersonic Jets," *AIAA Journal*, Vol. 37, No. 6, 1999, pp. 700–707.

[3]Miles, R. B., and Lempert, W., "Two-Dimensional Measurement of Density, Velocity, and Temperature in Turbulent High-Speed Air Flows by UV Rayleigh Scattering," *Applied Physics B*, Vol. 51, No. 1, 1990, pp. 1–7.

[4]Seasholtz, R. G., "Instantaneous 2D Velocity and Temperature Measurements in High Speed Flows Based on Spectrally Resolved Rayleigh Scattering," AIAA Paper 95-0300, Jan. 1995.

[5]Forkey, J. N., Lempert, W. R., and Miles, R. B., "Accuracy Limits for Planar Measurements of Flow Field Velocity, Temperature and Pressure Using Filtered Rayleigh Scattering," *Experiments in Fluids,* Vol. 24, No. 2, 1998, pp. 151–162.

[6]Herrin, J. L., and Dutton, J. C., "Supersonic Base Flow Experiments in the Near Wake of a Cylindrical Afterbody," *AIAA Journal*, Vol. 32, No. 1, 1994, p. 77.

[7]CFD Research Corp., Huntsville, AL, URL: http://www.cfdrc.com/ [cited 16 April 2001].

[8]Eckbreth, A. C., *Laser Diagnostics for Combustion Temperature and Species*, 2nd ed., Gordon and Breach, Amsterdam, 1996.

[9]McIntyre, T. J., Houwing, A. F. P., Palma, P. C., Rabbath, P., and Fox, J. S., "Imaging of Combustion in Supersonic Combustion Ramjet," *Journal of Propulsion and Power*, Vol. 13, No. 3, 1997, pp. 388–394.

[10]Palma, P. C., McIntyre, T. J., and Houwing, A. F. P., "PLIF Thermometry in Shock Tunnel Flows Using a Raman-Shifted Tunable Excimer Laser," *Shock Waves Journal*, Vol. 8, No. 5, 1998, pp. 275–284.

[11]Palma, P. C., "Laser-Induced Fluorescence Imaging in Free-Piston Shock Tunnels," Ph.D. Dissertation, Physics Dept., Australian National Univ., Canberra, Australian Capital Territory, Australia, 1999, URL: http://www.anu.edu.au/Physics/aldir/publications/Palma_PhD_1999.pdf [cited 16 April 2001].

[12]Hiller, B., McDaniel, J. C., Rea, E. C., and Hanson, R. K., "Laser-Induced Fluorescence Technique for Velocity Field Measurements in Subsonic Gas Flows," *Optics Letters*, Vol. 8, Sept. 1983, pp. 474–476.

[13]Hiller, B., and Hanson, R. K., "Simultaneous Planar Measurements of Velocity and Pressure Fields in Gas Flows Using Laser-Induced Fluorescence," *Applied Optics*, Vol. 27, Jan. 1988, pp. 33–48.

[14]McDaniel, J. C., Hiller, B., and Hanson, R. K., "Simultaneous Multiple-Point Velocity Measurements Using Laser-Induced Iodine Fluorescence," *Optics Letters*, Vol. 8, Jan. 1983, pp. 51–53.

[15]McMillin, B. K., Palmer, J. L., and Hanson, R. K., "Temporally Resolved, Two-Line Fluorescence Imaging of NO in a Transverse Jet in a Supersonic Cross-Flow," *Applied Optics,* Vol. 32, No. 36, 1993, pp. 7532–7545.

[16]Palmer, J. L., and Hanson, R. K., "Single-Shot Velocimetry Using Planar Laser-Induced Fluorescence Imaging of Nitric Oxide," AIAA Paper 93-2020, June 1993.

[17]Paul, P. H., Lee, M. P., and Hanson, R. K., "Molecular Velocity Imaging of Supersonic Flows Using Pulsed Planar Laser-Induced Fluorescence of NO," *Optics Letters*, Vol. 14, May 1989, pp. 417–419.

[18]Allen, M., Davis, S., Kessler, W., Legner, H., McManus, K., Mulhall, P., Parker, T., and Sonnenfroh, D., "Velocity Field Imaging in Supersonic Reacting Flows Near Atmospheric Pressure," *AIAA Journal*, Vol. 32, No. 8, 1994, pp. 1676–1682.

[19]Klavuhn, K. G., Gauba, G., and McDaniel, J. C., "High-Resolution OH LIF Velocity Measurement Technique for High-Speed Reacting Flows," AIAA Paper 92-3422, July 1992.

[20]Hiller, B., Booman, R. A., Hassa, C., and Hanson, R. K., "Velocity Visualization in Gas Flows Using Laser-Induced Phosphorescence of Biacetyl," *Review of Scientific Instruments*, Vol. 55, Dec. 1984, p. 1964.

[21]Barker, P. F., Thomas, A. M., McIntyre, T. J., and Rubinsztein-Dunlop, H., "Velocimetry and Thermometry of Supersonic Flow Around a Cylindrical Body," *AIAA Journal*, Vol. 36, No. 6, 1998, pp. 1055–1060.

[22]Ribarov, L. A., Wehrmeyer, J. A., Batliwala, F., Pitz, R. W., and DeBarber, P. A., "Ozone Tagging Velocimetry Using Narrowband Excimer Lasers," *AIAA Journal*, Vol. 37, No. 6, 1999, pp. 708–714.

[23]Donohue, J. M., and McDaniel, J. C., "Computer-Controlled Multiparameter Flowfield Measurements Using Planar Laser-Induced Iodine Fluorescence," *AIAA Journal*, Vol. 34, No. 8, 1996, pp. 1604–1611.

[24]Stalker, R. J., "A Study of the Free-Piston Shock Tunnel," *AIAA Journal*, Vol. 5, Dec. 1967, pp. 2160–2165.

[25]McIntosh, M. K., "Computer Program for the Numerical Calculation of Frozen Equilibrium Conditions in Shock Tunnels," Dept. of Physics, Australian National Univ., Canberra, Australian Capital Territory, Australia, 1968.

[26]Vardavas, I. M., "Modelling Reactive Gas Flows Within Shock Tunnels," *Australian Journal of Physics*, Vol. 37, Jan. 1984, pp. 157–177.

[27]McMillin, B. K., "Instantaneous Two-Line PLIF Temperature Imaging of Nitric Oxide in Supersonic Mixing and Combustion Flowfields," Ph.D. Dissertation, Stanford Univ., Stanford, CA, May 1993.

[28]Palma, P. C., Danehy, P. M., Houwing, A. F. P., and Olejniczak, J., "PLIF Thermometry of a Free Piston Shock Tunnel Nozzle Flow," AIAA Paper 98-2703, June 1998.

R. P. Lucht
Associate Editor